Supporting Information

From benzyl to fluorenyl: Enhancing photostability and modulating optoelectronic properties of para-azaquinodimethanes

Walaa Zwaihed[a,b], François Maurel[c], Magali Allain[d], Guido. F Pauli[e], Clément Cabanetos[d], Marwan Kobeissi[b], Bruno Schmaltz[a*].

[a]Laboratoire de Physico-Chimie des Matériaux et des Electrolytes Pour l'Energie (PCM2E) EA6299, Université de Tours, 37200 Tours, France; *walaa.zwaihed@univ-tours.fr*
[b]Laboratoire Rammal Rammal, Equipe de Synthèse Organique Appliquée SOA, Faculté des Sciences 5, Université Libanaise, Boulevard Nabih Berri, Quartier des Universités, Nabatieh 6573/14, Lebanon, *mkobeissi@ul.edu.lb*
[c] Université Paris Cité, CNRS, ITODYS, 75013 Paris, France; *maurel@u-paris.fr*
[d] Univ Angers, CNRS, MOLTECH-Anjou, SFR MATRIX-2 Boulevard de Lavoisier - 49045 - ANGERS CEDEX 01. *magali.allain@univ-angers.fr, clement.cabanetos@univ-angers.fr*
[e] Pharmacognosy Institute and Department of Pharmaceutical Sciences, Retzky College of Pharmacy, University of Illinois
* Correspondence: *bruno.schmaltz@univ-tours.fr*

Table of Contents

1. Materials and Characterization Methods

All reactions were carried out in oven-dried glassware sealed with rubber septa under an inert atmosphere and were stirred using Teflon-coated magnetic stir bars. Triethylamine was distilled before use, and dry DMF over molecular sieves from Fisher Scientific was used for all reactions. All commercially available chemicals and solvents (dry and argon bubbled chloroform and dichloromethane solutions were used for UV and CV) were purchased from Sigma Aldrich, TCI Europe, Alfa Aesar, Acros Organics and Ficher Scientific and were used without further purification. Deuterated solvents were purchased from Eurisotop and used as received. All reactions were monitored by thin-layer chromatography (TLC) carried out on 0.25-mm silica gel plates (60 F-254) using UV light (254 nm, 365 nm) for visualization.

The ^{1}H and ^{13}C NMR spectra were recorded on a Bruker Avance FT-NMR-300 (^{1}H: 300 MHz, ^{13}C: 75 MHz). Chemical shifts (δ) are reported in parts per million (ppm) and all coupling constants (*J*) are expressed in Hertz (Hz). The spectra were referenced to the residual protons of the deuterated solvent (DMSO d_6: 2.500 ppm for ^{1}H NMR and 39.52 ppm for ^{13}C NMR; THF d_8: 3.580 ppm for ^{1}H NMR and 67.21 for ^{13}C NMR). The following abbreviations have been used for the NMR assignment: s for singlet, d for doublet, t for triplet, and m for multiplet. The raw NMR data are shared via nmrXiv.org: https://nmrxiv.org/project/Vf4FLFcWvrYQJdmTs1orDBnK27oQq3gqsB3sGWhz. Mass spectra were recorded on a Finnigan MAT 8500 using an ionization energy of 70 eV (electron impact).

HifSA analysis was performed using the Cosmic Truth software (ctm.nmrsolutions.fi) by NMR Solutions (Kuopio, Finland). The generation of these detailed ^{1}H NMR fingerprints followed an established protocol,[1,2] briefly summarized as follows: The experimental NMR spectra were imported as JDX files, the structures of the compounds under study were input as SDF files to generate starting spin parameters. Subsequent iterative calculation yielded the true spectral parameters of the experimental spectra and creates a link between the 3D chemical structures of the analyzed compounds and their definitive ^{1}H NMR assignments (HifSA profiles and fingerprints).

The UV-Visible spectra were recorded with a Jasco V-670 spectrometer. The emission spectra were recorded with fluoro-max-4 from Horiba. The measurements were conducted in 10^{-5}M $CHCl_3$ solution. Cyclic voltammetry (CV) was performed on a Biologic Applied Research MPG2 multi-channel potentiostat, and CV experiments were performed at room temperature with a conventional three-electrode setup consisting of a platinum disk working electrode, silver wire and platinum wire, respectively, as reference and counter electrodes. The potential of the reference electrode was calibrated using Fc/Fc^{+} couple as an internal standard. All the measurements were conducted in anhydrous dichloromethane media under argon atmosphere using Bu_4NClO_4 (0.1 M) as a supporting electrolyte. Differential scanning calorimetry (DSC) measurements were performed on Perkin-Elmer DSC-4000 (heating/cooling rate of 10 °C/min). Thermogravimetric analysis (TGA) was fulfilled using a Perkin Elmer STA 6000 at a heating rate of 10 °C/min under N_2. Melting point determination by the capillary method was performed by Stuart Scientific SMP3 Melting Point Apparatus.

2. XRD Data

Crystal data for **F-AQM** were collected on a Rigaku Oxford Diffraction SuperNova diffractometer equipped with an Atlas CCD detector and micro-focus Cu-Kα radiation (λ = 1.54184 Å). The structure was solved by dual-space algorithm and refined on F2 by full matrix least-squares techniques using SHELX package (G.M. Sheldrick, ShelXT-2018/2, ShelXL-2018/3). All non-hydrogen atoms were refined anisotropically and the H atoms were included at calculated position and refined using a riding

model. Multiscan empirical absorption was corrected by using CrysAlisPro program (CrysAlisPro, Rigaku Oxford Diffraction, V1.171.41.118a, 2021). Deposition Number 2463879 contains the supplementary crystallographic data for this paper. These data are provided free of charge by the joint Cambridge Crystallographic Data Centre and Fachinformationszentrum Karlsruhe Access Structures service.

Crystallographic data for **F-AQM** : $C_{42}H_{42}N_2O_2$, M = 606.77, red prism, 0.378 x 0.180 x 0.095 mm^3, Triclinic, space group *P*-1, a = 7.5529(2) Å, b = 14.0354(4) Å, c = 16.8483(5) Å, α = 110.038(2)°, β = 98.621(2)°, γ = 90.387(2)°, V = 1655.73(8) $Å^3$, Z = 2, ρcalc = 1.217 g/cm^3, μ = 0.575 mm^{-1}, F(000) = 648, θmin = 2.829°, θmax = 76.220°, 13789 reflections collected, 6668 unique (R_{int} = 0.0235), parameters / restraints = 417 / 0, R1 = 0.0418 and wR2 = 0.1125 using 5865 reflections with I>2σ(I), R1 = 0.0467 and wR2 = 0.1180 using all data, GOF = 1.029, -0.161 < Δρ < 0.216 e.$Å^{-3}$.

All π-stacking distances were measured in the following way: least-squares planes were calculated from the atoms in the backbone of **F-AQM**. The perpendicular distance between adjacent planes was then calculated from the equations of the planes.

3. Computational details

All the calculations have been performed with Gaussian16. B.01 program applying default algorithms and convergence thresholds[3]. The ground-state geometries of the studied compounds were optimized by using the PBE0 functional in combination with the 6–311G(d,p) basis set. Frequency calculation was then carried out at the same level of theory to ensure the energy of the optimized geometry corresponding to the true minima on the potential energy surface. The effect of the solvent was considered through the integral equation formalism polarizable continuum model (EFPCM) with the parameters of chloroform as the solvent. To simulate the optical properties, from the ground state optimized geometries at the PBE0/6-311G(d,p) level, the lowest-lying singlet states were considered and vertical energies excitation were calculated in the frame of time dependent density functional theory (TD-DFT) using the ωB97XD functional cconsidering its accuracy with the experimental data.

To study the interaction of the molecules in the X-ray structures as well as in solution, we studied the dimer complex formed by the interaction between two **F-AQM** molecules. The starting geometry was taken from X-ray crystal structures and the optimized structure of resulting dimer is shown in Fig. 4. For the dimer, calculation included the dispersion correction (D3 correction) introduced by Grimme[4] to properly describe weak interactions, taking into account dispersion forces. The interaction energy within the complexes was calculated as the difference of the total energy of the complex and the sum of the energies of the isolated monomers (see below). The interaction energy was corrected for the inherent basis set superposition error (BSSE) using the Boys–Bernardi[5] counterpoise technique over the optimized geometry.

The energy of complexation was calculated according to the relation:

$$\mathbf{\Delta E_{Complexation} = E_{dimer} - 2\ E_{monomer}}$$

Where $\Delta E_{complexation}$ is the complexation energy, E_{dimer}, and $E_{monomer}$ are respectively the full relaxed energies of the formed complex and the free monomer.

To obtain a visual representation of the interaction in the dimer, the noncovalent interaction (NCI) index, based on the reduced gradient of the electron density[6], was calculated to identify attractive and repulsive interactions. In the resulting plot, the strength of interactions is depicted as color codes: red surfaces indicate strong repulsions, green surfaces show weak interactions, and blue surfaces signify strong attractions.

The isosurface plots were calculated with Multiwfn (version 3.8) program[7] and their graphical representation was visualized in VMD1.9.3[8].

4. Experimental procedures

*Synthesis of intermediates **A** and **B** by Knoevenagel condensation*

A: (**2a** in ref.9): For the synthesis and NMR characterization of **A**, please refer to[9].

B: Into a mixture of 1,4-Diacetyl-2,5-piperazinedione (1 eq, 5 mmol) 9H- fluorenone (2.3 eq, 11.6 mmol), in DMF (24 mL) was syringe injected triethylamine (4 eq, 20 mmol) at 120 ◦C under argon. Upon addition, the original yellow solution turned dark red. The reaction was stopped after 24 h, cooled down to room temperature and placed in ice-cold water. The red precipitate formed was collected by filtration and rinsed with water, DCM and methanol. The solid obtained was pure enough for the next step without chromatography. (1.09 g, 50% yield). (^{1}H NMR, DMSO d_6, 300MHz): δ = 11.39 (s, 2H), 8.83 (d, *J* = 7.7 Hz, 2H), 8.07 (d, *J* = 7.8 Hz, 2H), 7.89 – 7.79 (m, 4H), 7.48 – 7.22 (m, 8H). (^{13}C NMR, DMSO d_6, 75 MHz): δ=161.99, 140.32, 139.94, 136.00, 134.78, 129.45, 129.30, 127.61, 126.73, 119.95, 119.78, 39.52. HRMS: M+1 found= 439.14357, theoretical= 439.14410.

Synthesis of target p-AQM molecules by alkylation

For the synthesis of **AQM1**, please refer to[9]. (^{1}H NMR, THF-d_8, 300 MHz): δ= 8.12 (d, *J* = 8.6 Hz, 4H), 7.33 (t, *J* = 7.4 Hz, 4H), 7.23 (t, *J* = 6.7 Hz, 2H), 6.89 (s, 2H), 4.44 (t, *J* = 6.7 Hz, 4H), 1.98 – 1.83 (m, 4H), 1.43 (m, 12H), 0.94 (t, *J* = 5.4 Hz, 6H). (^{13}C NMR, THF-d_8, 75 MHz): δ= 158.88, 136.96, 131.97, 131.03, 128.70, 128.62, 123.08, 67.21, 66.92, 66.62, 32.41, 29.38, 26.72, 25.66, 25.39, 25.13, 24.86, 24.59, 23.34, 14.30, 14.20. HRMS: M + 1 found 459.30, theoretical: 459.63.

F-AQM: A mixture of intermediate **B** (1 eq, 2 mmol), K_2CO_3 (5 eq, 10 mmol) and 1-bromohexane (4 eq, 8 mmol) in DMF (10 mL) was stirred at 100 ◦C for 2 h under argon atmosphere. A change of colour from red to dark pink was detected and a precipitate was formed in the reaction mixture. After cooling to room temperature, the reaction mixture was placed in ice bath for 1h. Then, the precipitate formed was filtered and washed with methanol to afford the desired product as a violet solid (0.85 g, 70% yield). (^{1}H NMR, THF-d_8, 300 MHz): δ= 8.99 – 8.88 (m, 2H), 8.03 (d, *J* = 7.8 Hz, 2H), 7.75 – 7.65 (m, 4H), 7.37 – 7.21 (m, 6H), 7.16 (td, *J* = 7.8, 1.2 Hz, 2H), 4.68 (t, *J* = 6.6 Hz, 4H), 2.00 – 1.86 (m, 4H), 1.60 – 1.27 (m, 12H), 0.89 (t, *J* = 7.0 Hz, 6H). (^{13}C NMR, THF-d_8, 75 MHz): δ= 159.81, 142.10, 141.34, 140.04, 137.22, 132.34, 130.72, 129.68, 129.11, 127.95, 127.56, 126.90, 119.93, 69.05, 67.21, 32.40, 29.15, 26.94, 23.28, 14.19. HRMS: M+1 found= 607.33105, theoretical= 607.33191.

5. NMR analysis of F-AQM

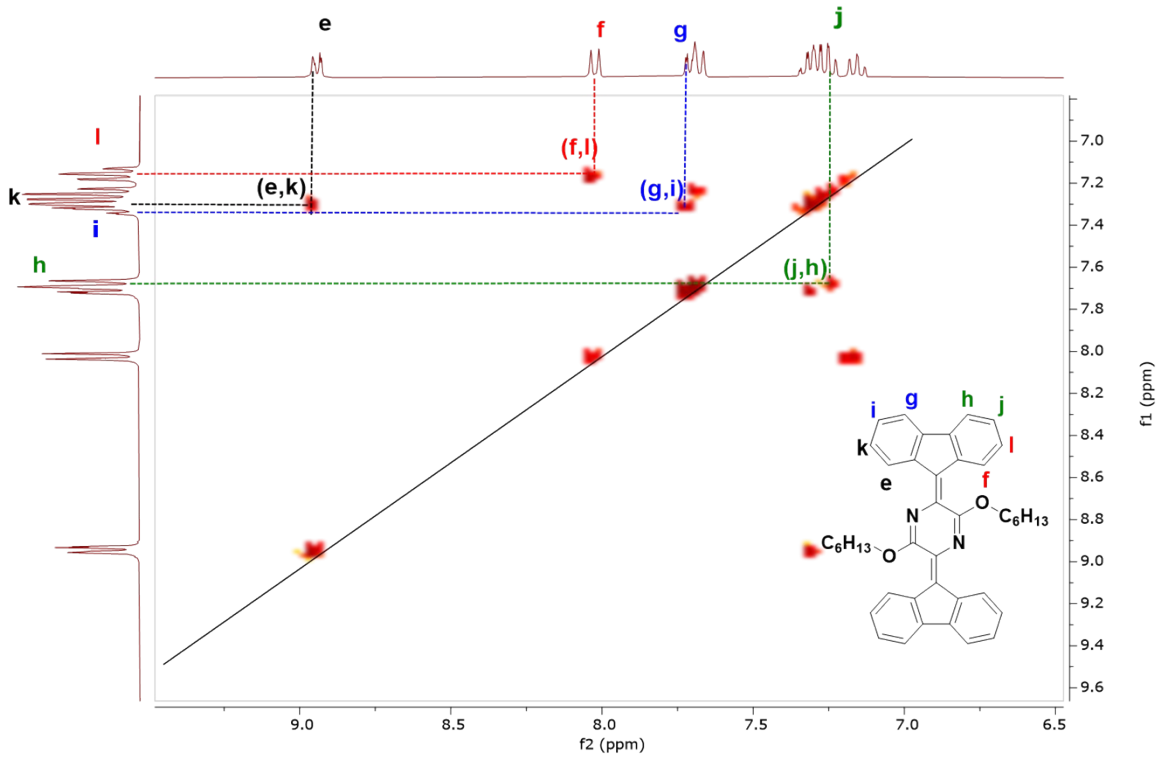

Fig. S1: ^{1}H-^{1}H COSY 2D NMR spectrum of **F-AQM** (300 MHz, THF-d_8) in the aromatic region (6.50 to 9.00 ppm)

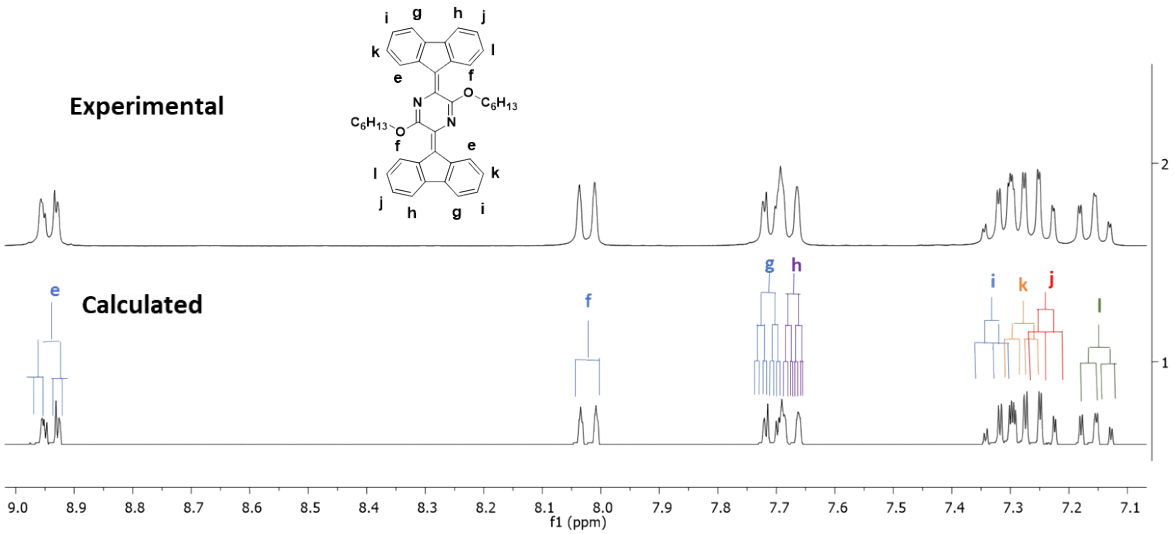

Fig. S2: Comparison between the experimental (THF d_8 at 300 MHz) and calculated (HifSA) spectra of **F-AQM**. The coupling trees are simplified first-order representation of the actual higher-order peak patterns.

Table S1: Comparison of the chemical shifts (δ) and coupling constants (*J*) obtained experimentally from the ^{1}H NMR spectrum in THF d_8 via HifSA (Cosmic Truth [CT]software, NMR Solutions).

F-AQM	δ (ppm)		*J* (Hz)	
	Experimental	**Calculated**	**Experimental**	**Calculated**
$\mathbf{H_e}$	8.94	8.9522	m	$^{3}J_{He\text{-}Hk}$=7.92
$\mathbf{H_f}$	8.03	8.0329	$^{3}J_{Hf\text{-}Hl}$= 7.8	$^{3}J_{Hf\text{-}Hl}$= 8.03
$\mathbf{H_g}$	7.71	7.7179	m	$^{3}J_{Hg\text{-}Hi}$= 7.55, $^{4}J_{Hg\text{-}Hk}$= 1.19
$\mathbf{H_h}$	7.70	7.6863	m	$^{3}J_{Hh\text{-}Hj}$= 7.57, $^{4}J_{Hh\text{-}Hl}$= 1.19
$\mathbf{H_i}$	7.29	7.3265	m	$^{3}J_{Hi\text{-}Hg}$= 7.55, $^{3}J_{Hi\text{-}Hk}$= 7.41, $^{4}J_{Hi\text{-}He}$= 1.07
$\mathbf{H_k}$	7.28	7.2903	m	$^{3}J_{Hk\text{-}He}$= 7.92, $^{4}J_{Hk\text{-}Hg}$= 1.19
$\mathbf{H_j}$	7.27	7.2598	m	$^{3}J_{Hj\text{-}Hh}$= 7.57, $^{3}J_{Hj\text{-}Hl}$= 7.35
$\mathbf{H_l}$	7.16	7.1674	m	$^{3}J_{Hl\text{-}Hf}$= 8.03, $^{3}J_{Hl\text{-}Hj}$= 7.35

6. XRD analysis

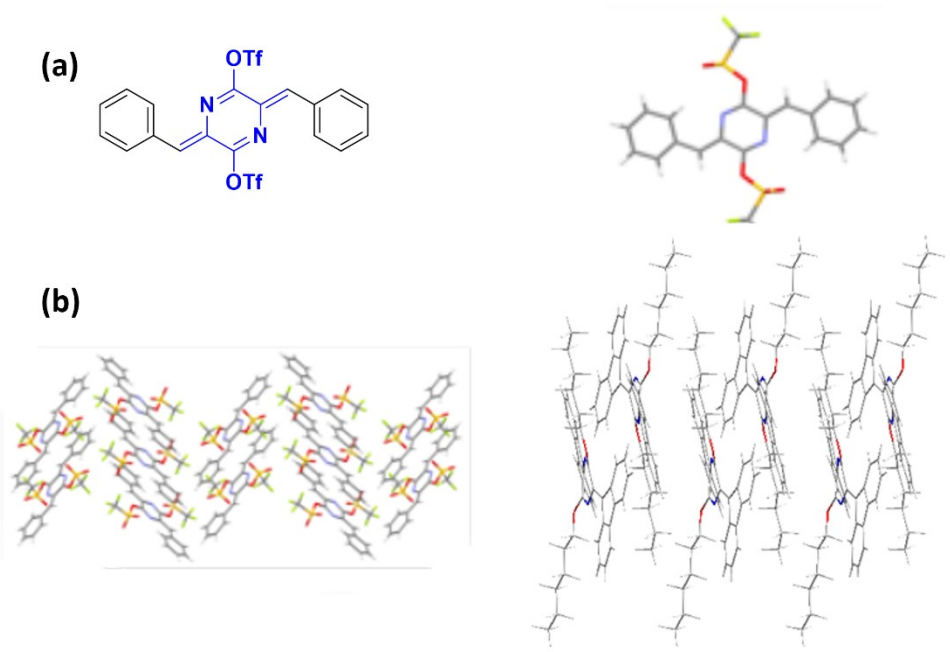

Fig. S3: (a) Stick representations of X-ray crystallographic structure of **monomer 1.** [10] (b) Molecular packing diagram of **monomer 1** (bottom left) [10] and **F-AQM** (bottom right).

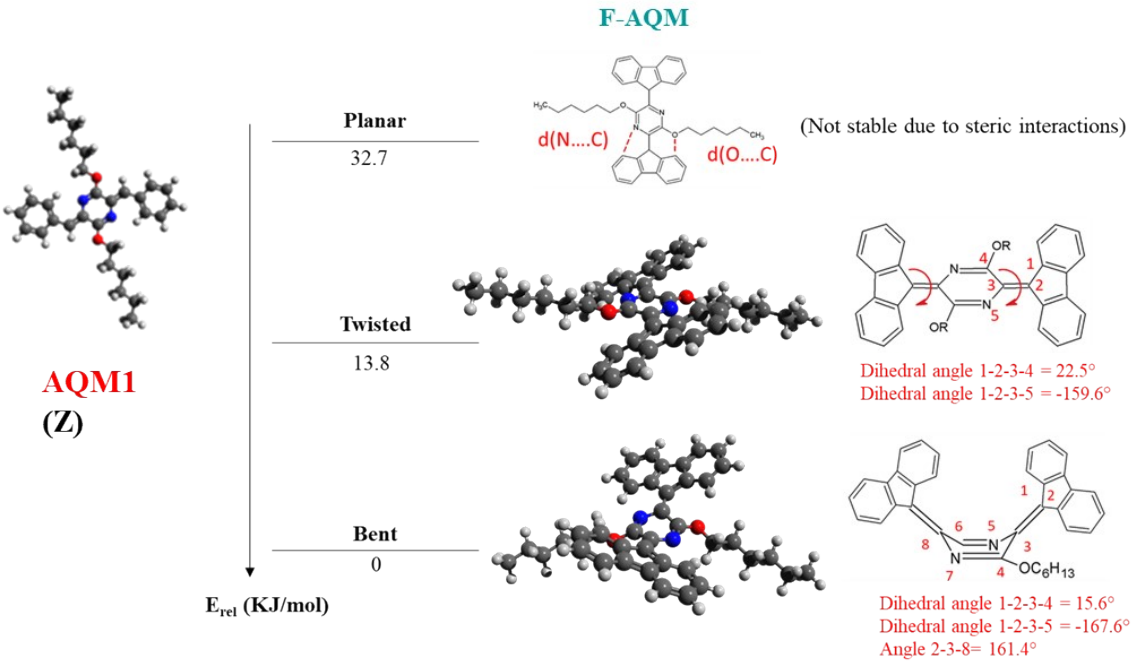

7. DFT Calculations

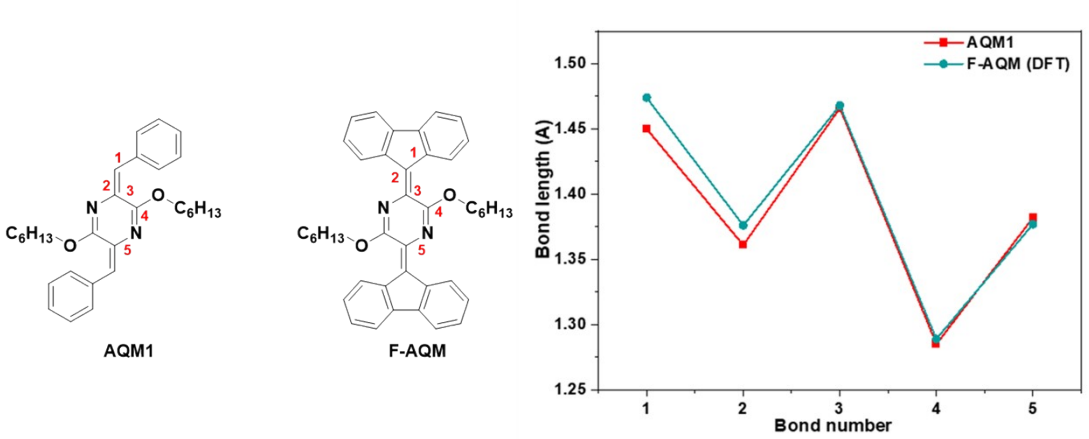

Fig. S4: Optimized geometries of the most stable isomer of **AQM1** (Z) and the three possible conformations of **F-AQM**, with planar being the least stable due to repulsive interactions (shown in red)

Fig. S5: Plots of carbon–carbon bond length for bonds 1 to 5 in **AQM1** and **F-AQM**.

Table S2. Experimental and calculated (PBE0-GD3/6-311G(d,p)) bond length (in Å) and dihedral angles (in °) of compound **F-AQM**

	Exptl*	Calc	
		Monomer**	Monomer in the dimer
1-2	1.485	1.474	1.472
2-10	1.485	1.473	1.470
2-3	1.382	1.376	1.376
3-4	1.470	1.466	1.461
4-5	1.287	1.286	1.285
5-6	1.381	1.376	1.376
6-7	1.378	1.376	1.381
7-8	1.481	1.473	1.479
7-9	1.481	1.474	1.479
1-2-3-4	-6.7	-15.5	-11.5
10-2-3-11	-6.6	-11.9	-11.5
8-7-6-5	-12.1	-11.9	-2.33
9-7-6-12	-14.3	-15.5	-8.13
MSE[a]		-1.166	0.476

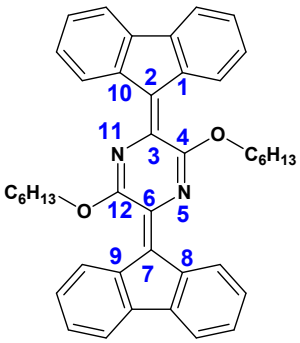

* This work
** bent conformation
[a] Mean Signed Error

The dimer formed by the interaction of two **F-AQM** monomer units exhibits a center of symmetry (point group Ci), consistent with experiment. However, due to the intermolecular interactions within the dimer, each monomer adopts a slightly distorted geometry and loses its individual symmetry. For example, the carbon-carbon double bonds between 2-3 and 6-7 are calculated to be 1.376 Å and 1.381 Å, respectively. The resulting bond lengths difference of 0.005 Å is in excellent agreement with experiment value of 0.004 Å.

7.1. Geometry optimization

The resulting basis set superposition error (BSSE)[4,11]-corrected interaction energy was determined as -126.1 kJ.mol-1 for the complex optimized from the X-ray structure, i.e., in gas phase, and -124.5 kJ.mol-1 for the complex optimized in $CHCl_3$. In the dimer, a proximity between the fluorenyl and para-azaquinodimethane cores was found. While it is perceivable that dimerization may affect the solution NMR spectra, the effects are likely very subtle. As suggested by the HifSA profiles (Fig. S2), these effects were included in the achievable natural line width of the spectra.

8. Thermal Properties

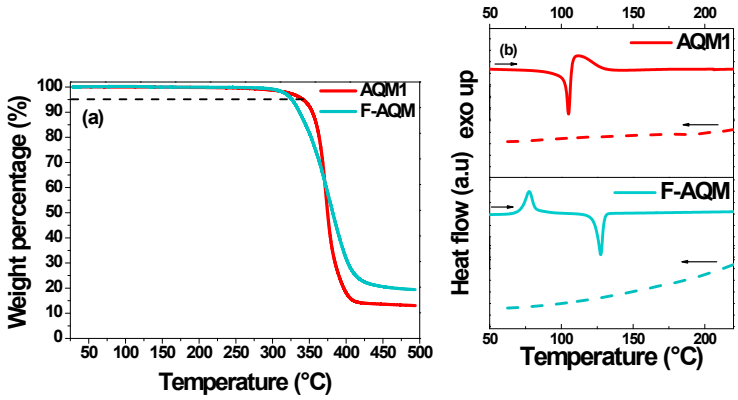

Fig.S6: (a) TGA curves under nitrogen at 10°C/min scan rate. (b) DSC curves under nitrogen at 10°C/min scan rate, first heating (full line) and cooling (dashed line) scans.

9. Electrochemical properties

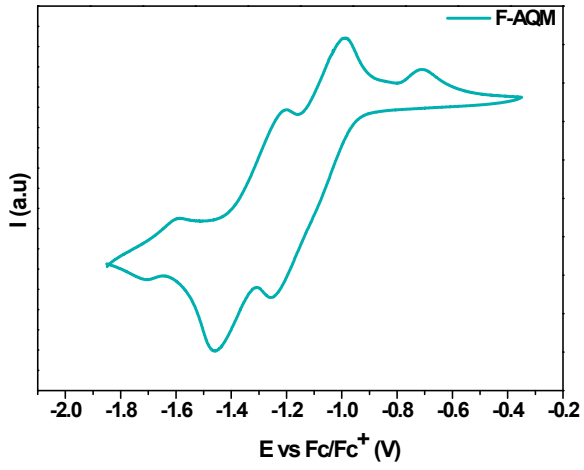

Fig.S7: Cyclic voltammogram of **F-AQM** (cathodic scan) in 10^{-2}M CH_2Cl_2 solutions containing 0.1 M tetrabutylammonium perchlorate as supporting electrolyte at 50 mV/s scan rate.

Fig.S8:

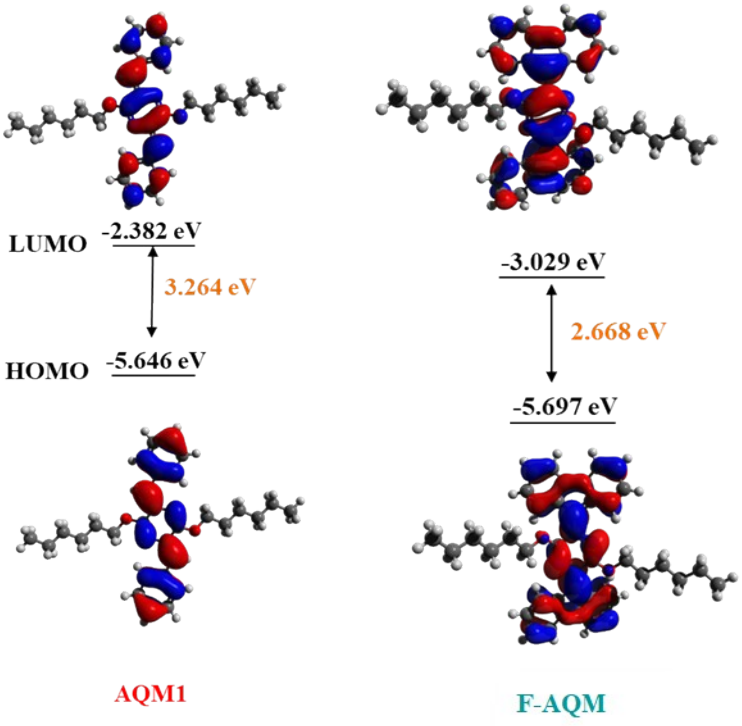

Calculated molecular orbital distribution and energy levels of p-AQM molecules (HOMO, LUMO and HOMO-LUMO gap in eV).

10. Absorption properties

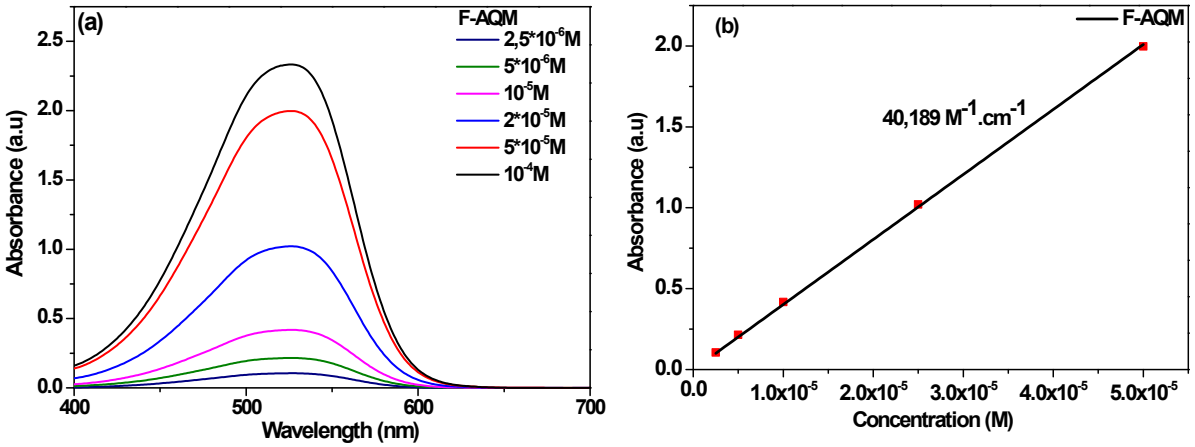

Fig. S9: (a) UV/visible absorption spectra of **F-AQM** at different concentrations in $CHCl_3$ (b) Absorbance vs Concentration plot of **F-AQM** in $CHCl_3$.

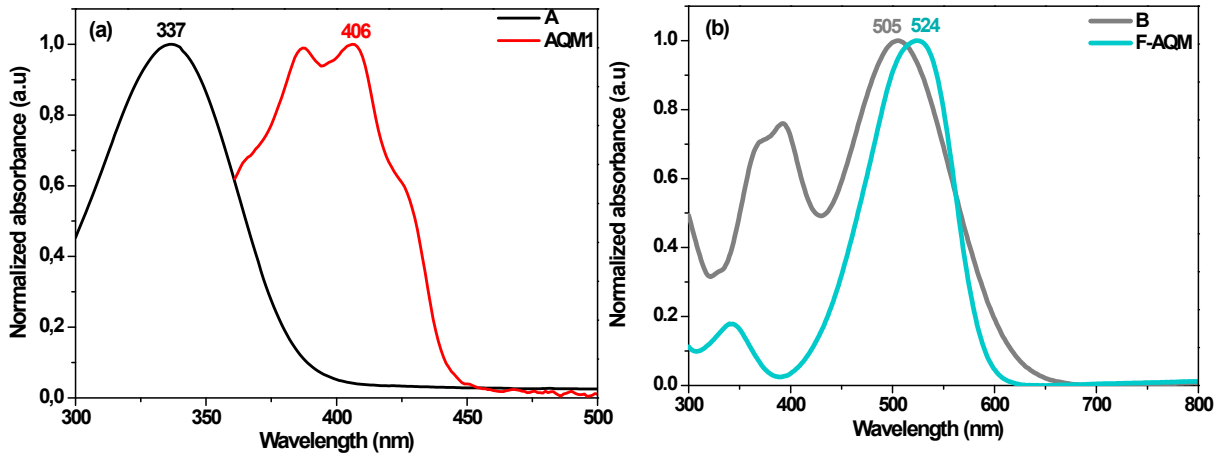

Fig. S10: Comparison of normalized UV/visible absorption spectra of non-quinoidal intermediates and target molecules: (a) **A** and **AQM1** in 10^{-5}M THF solution, (b) **B** and **F-AQM** in 10^{-5} M DMF solution.

Table S3: Optical, electrochemical and thermal data of **AQM1** and **F-AQM**

	λ_{max} (nm) (sol)	λ_{max} (nm) (film)	λ_{onset} (nm) (sol)	$E_{opt}^{g\ a}$ (eV) (sol)	ε^b ($M^{-1}.cm^{-1}$) $\times 10^4$	E_{ox} (eV)	$E_{HOMO}{}^c$ (eV)	$E_{LUMO}{}^d$ (eV)	Td (°C)	Tm^e (°C)	Tm^f (°C)
AQM1	406	408	450	2.75	2.2	0.72	-5.82	-3.07	340	105	109
F-AQM	525	534	593	2.09	4.0	0.89	-5.99	-3.90	327	127	155

[a] optical band gap calculated from onset of absorption in solution according to the following equation: $E_{opt}^{g} = \frac{1240}{\lambda onset}$. [b] extinction coefficient in $CHCl_3$. [c] HOMO energy level calculated using equation $E_{HOMO} = -e(E_{ox} + 5.1eV)$. [d] LUMO energy level calculated using equation $E_{LUMO} = E_{HOMO} + E_g^{opt}\ (solution)$. [e] melting temperatures determined from DSC scans, [f] melting temperatures determined by capillary method.

11. TD-DFT calculations

Table S4. Wavelength (λ in nm), oscillator strength (*f*) and molecular orbitals implied in the main electronic transitions of **A**, **AQM1**, **B** and **F-AQM** (bent geometry) for the UV-vis region (TD-DFT calculations at the wb97xd/6-311G(d,p)//pbe1pbe/6-311g(d,p) level).

Theoretical λ (in nm)	*f*	Exptl	Assignment	
A				
323	1.565	337	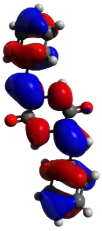 HOMO	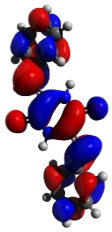 LUMO
AQM1				
400	1.565	406	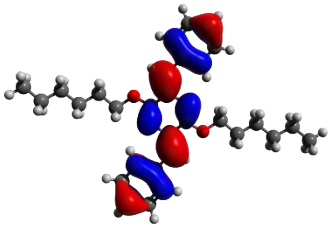 HOMO	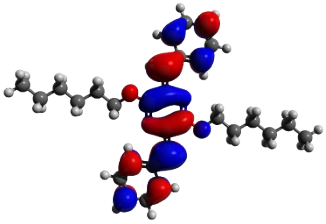 LUMO
220	0.316		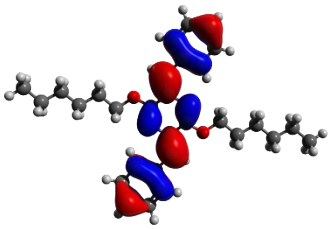 HOMO	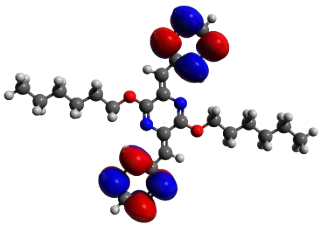 LUMO+3
B				
425	1.455	505	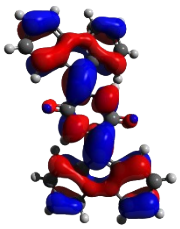 HOMO	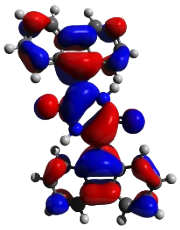 LUMO
F-AQM				
514	1.297	525	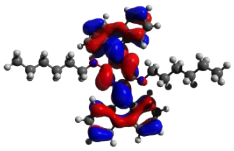 HOMO	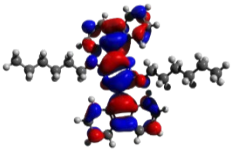 LUMO

315	0.156	343	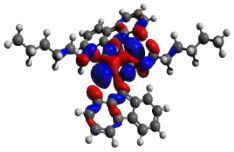	
			HOMO-6	LUMO

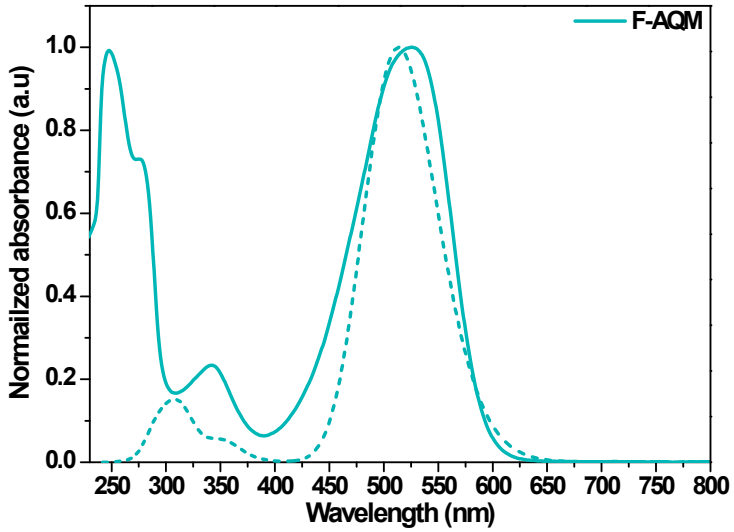

Fig. S11: TD-DFT calculations (wb97xd/6-311G(d,p)//pbe1pbe/6-311g(d,p) level of calculations) of the absorption spectra of **F-AQM** geometry-(bent line) and dotted line), to the comparison UV experimental spectrum (full line).

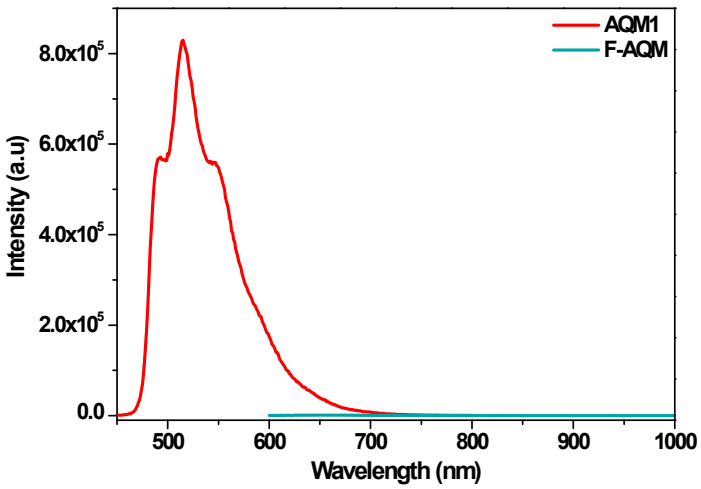

12. Emission properties

Fig.S12: PL emission spectra of **AQM1** and **F-AQM**, excited at 425 nm and 525 nm respectively.

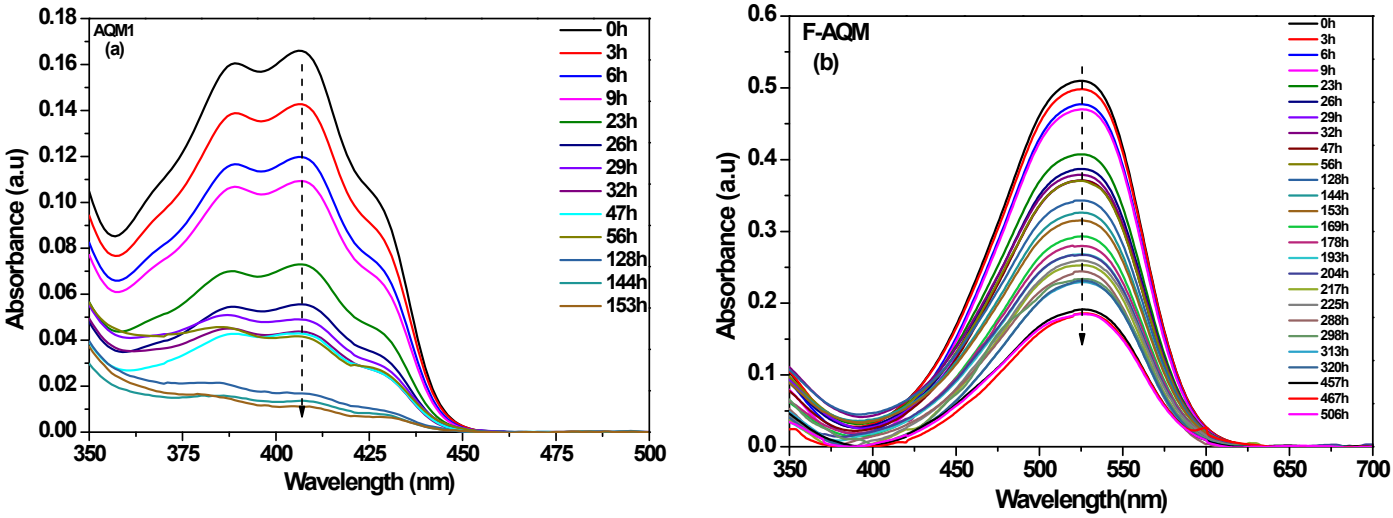

13. Photostability experiments

Fig. S13: Changes of absorption spectra of (a) **AQM1** and (b) **F-AQM** in $CHCl_3$ solution ($\sim 10^{-5}$ M) under ambient light and air conditions.

14. NMR spectra

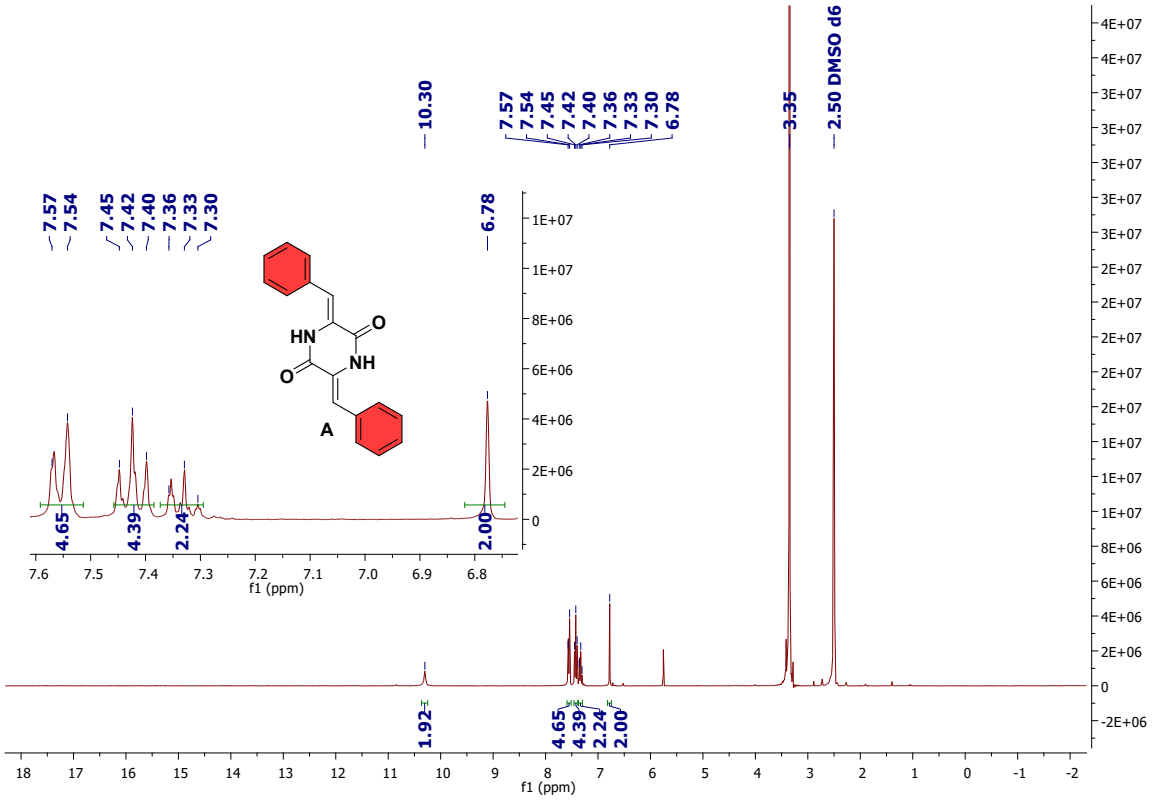

Fig. S14: [1] H NMR spectrum of **A** (DMSO d_6, 300 MHz)

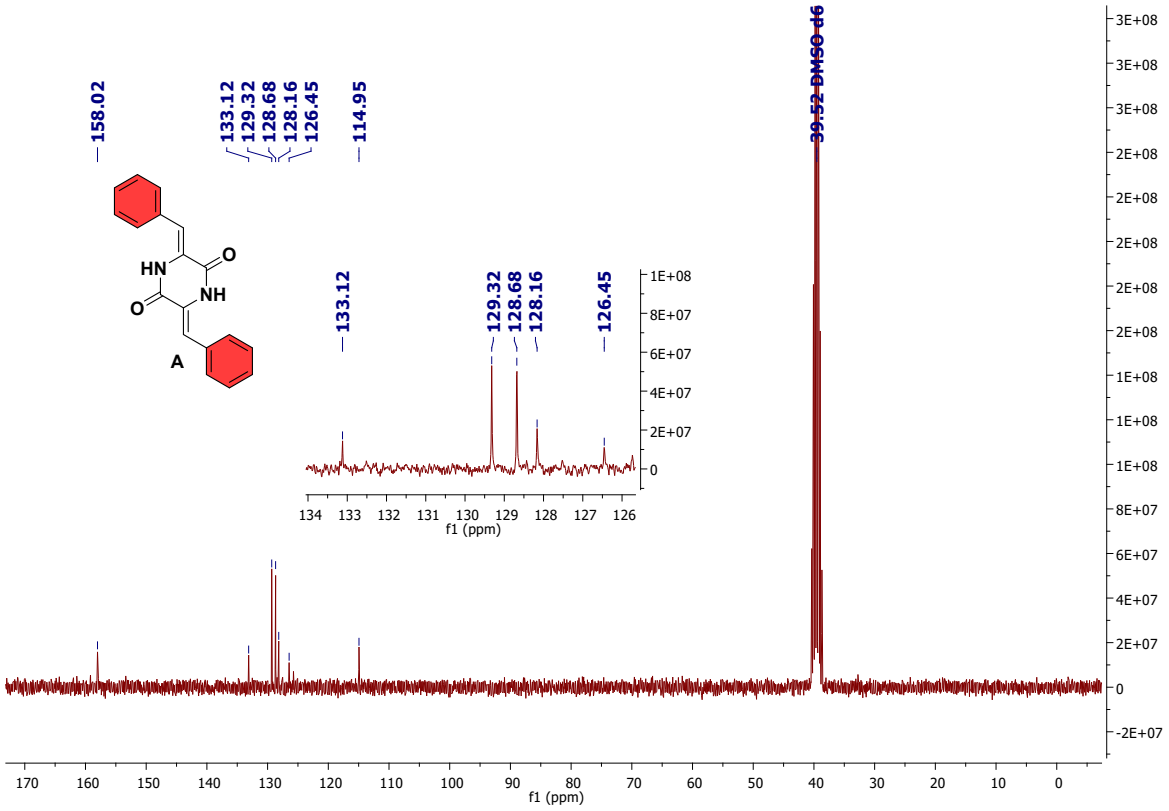

Fig. S15: [13]C NMR spectrum of **A** (DMSO d_6, 75 MHz)

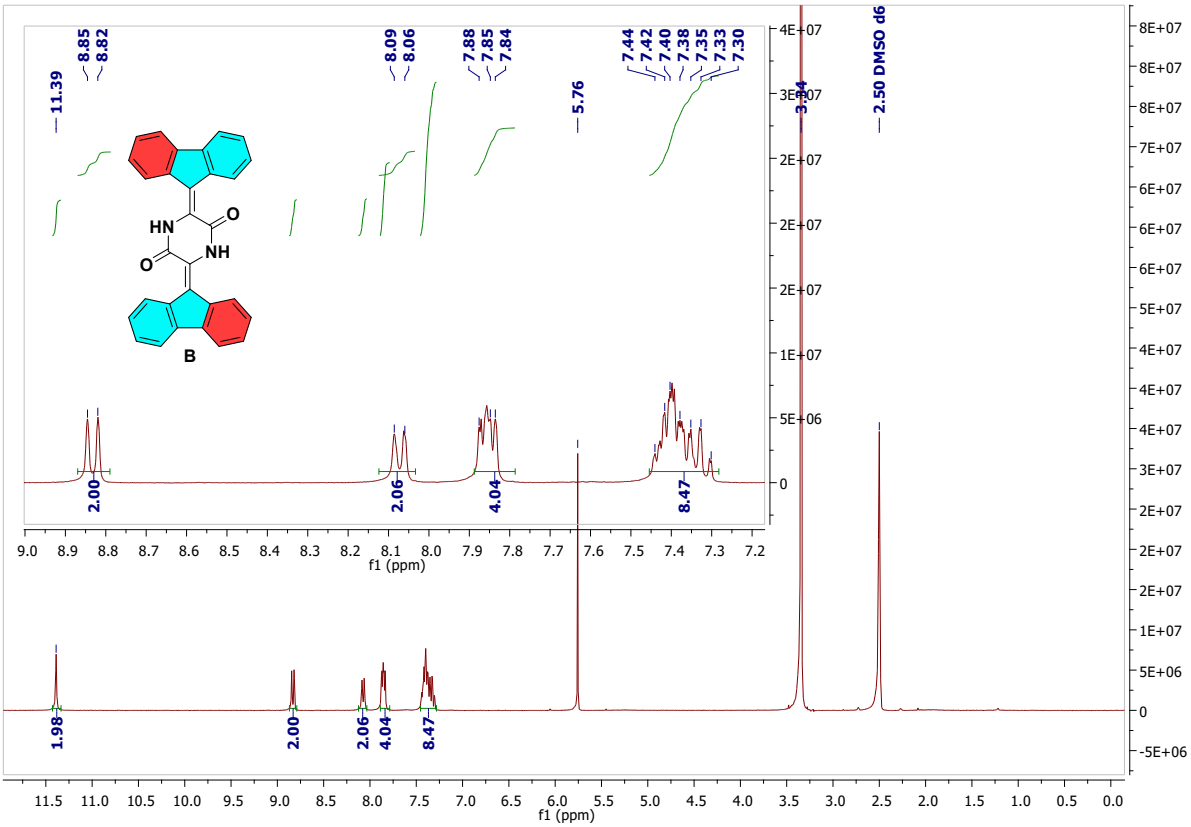

Fig. S16: [1] H NMR spectrum of **B** (DMSO d_6, 300 MHz)

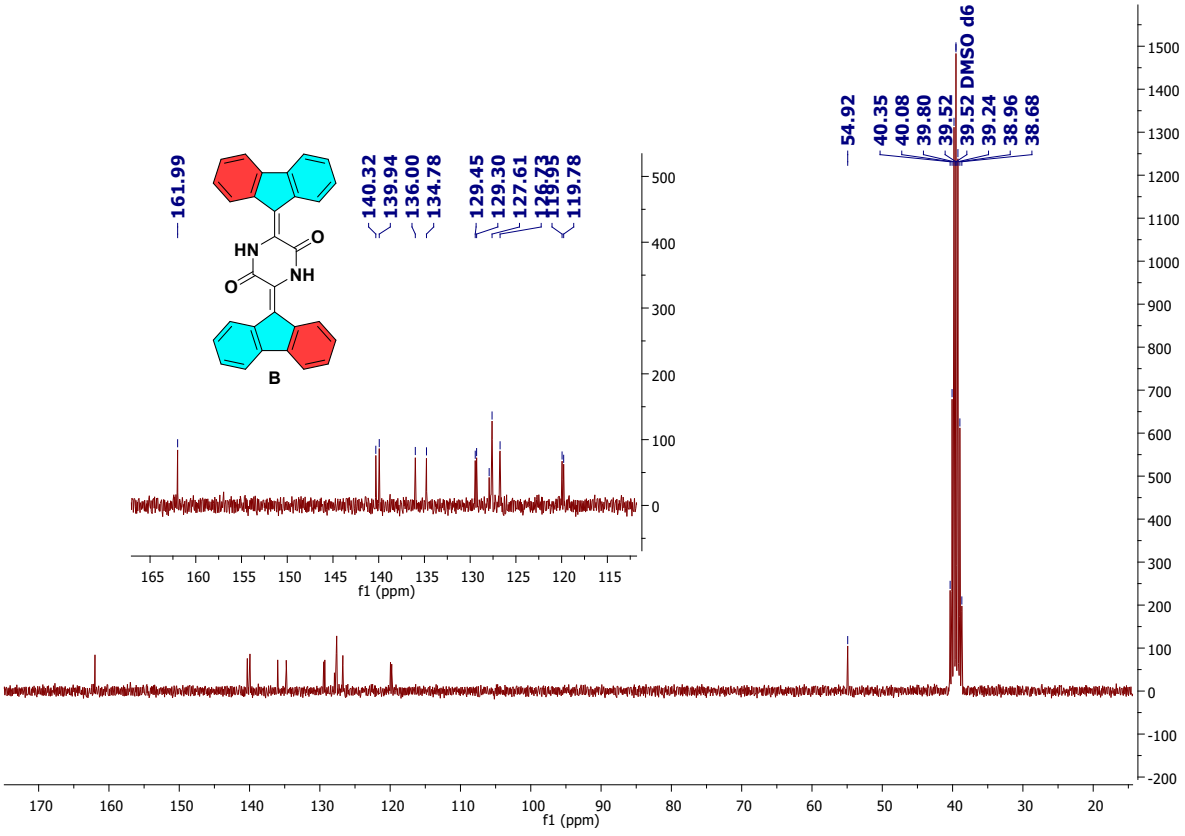

Fig. S17: [13] C NMR spectrum of **B** (DMSO d_6, 75 MHz)

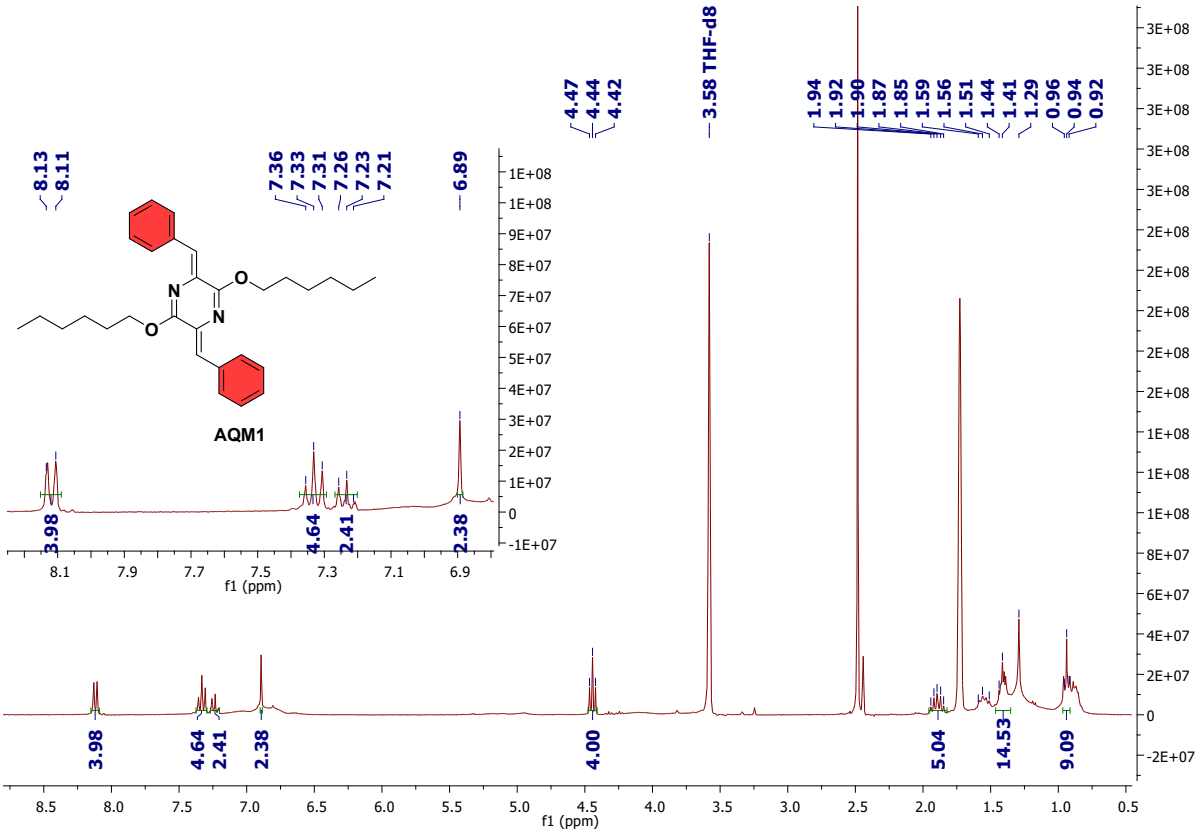

Fig. S18: [1] H NMR spectrum of **AQM1** (THF d_8, 300 MHz)

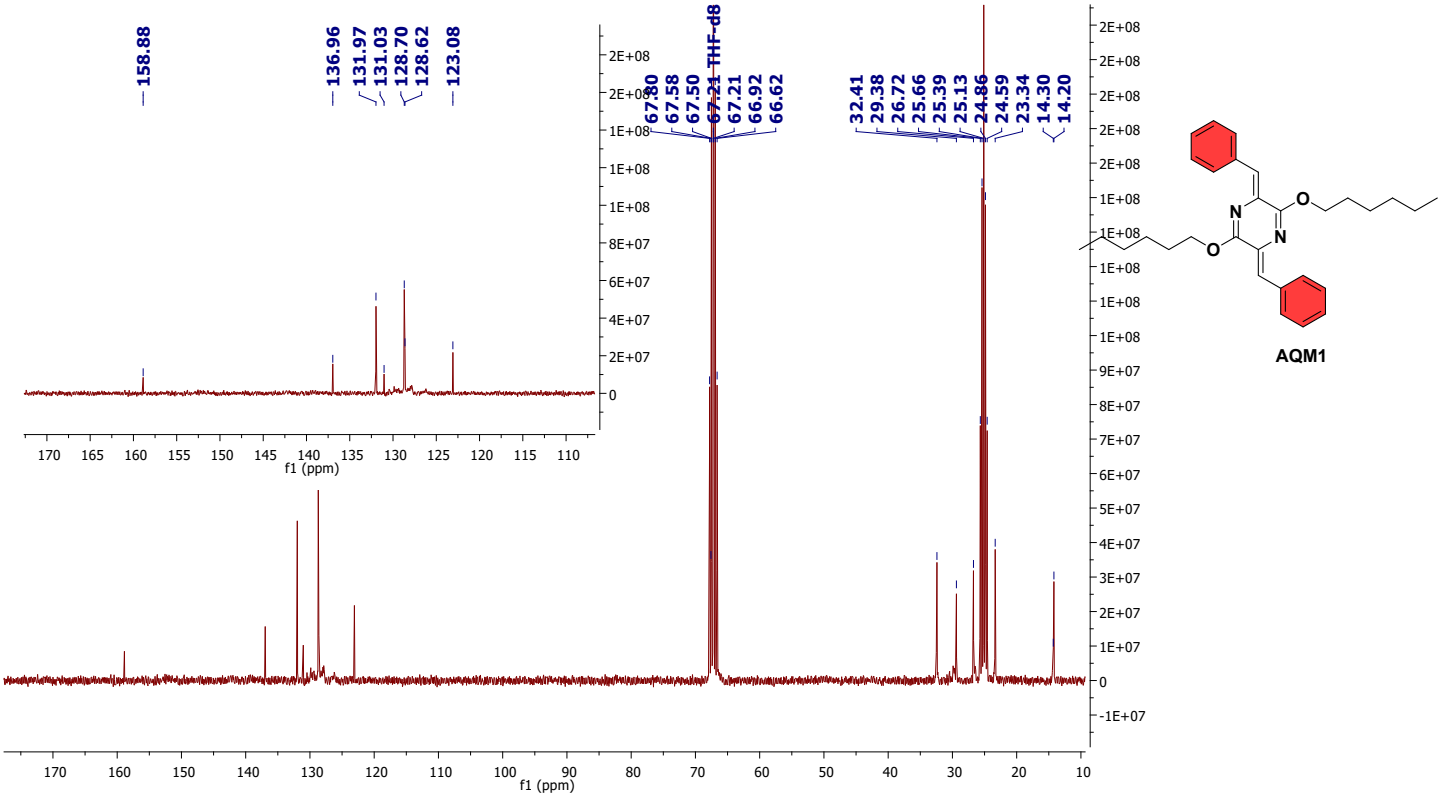

Fig. S19: ^{13}C NMR spectrum of **AQM1** (THF d_8, 75 MHz)

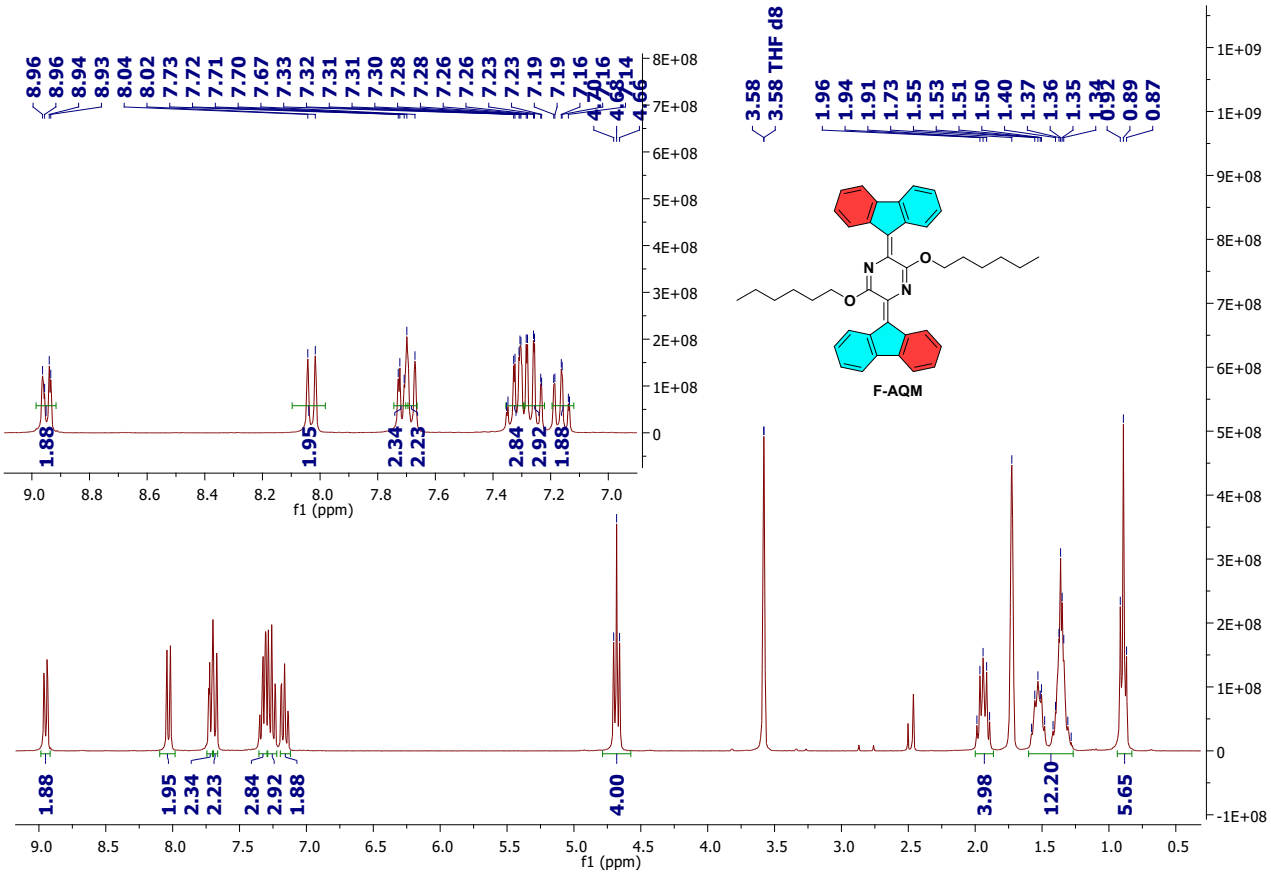

Fig. S20: ^{1}H NMR spectrum of **F-AQM** (THF d_8, 300 MHz)

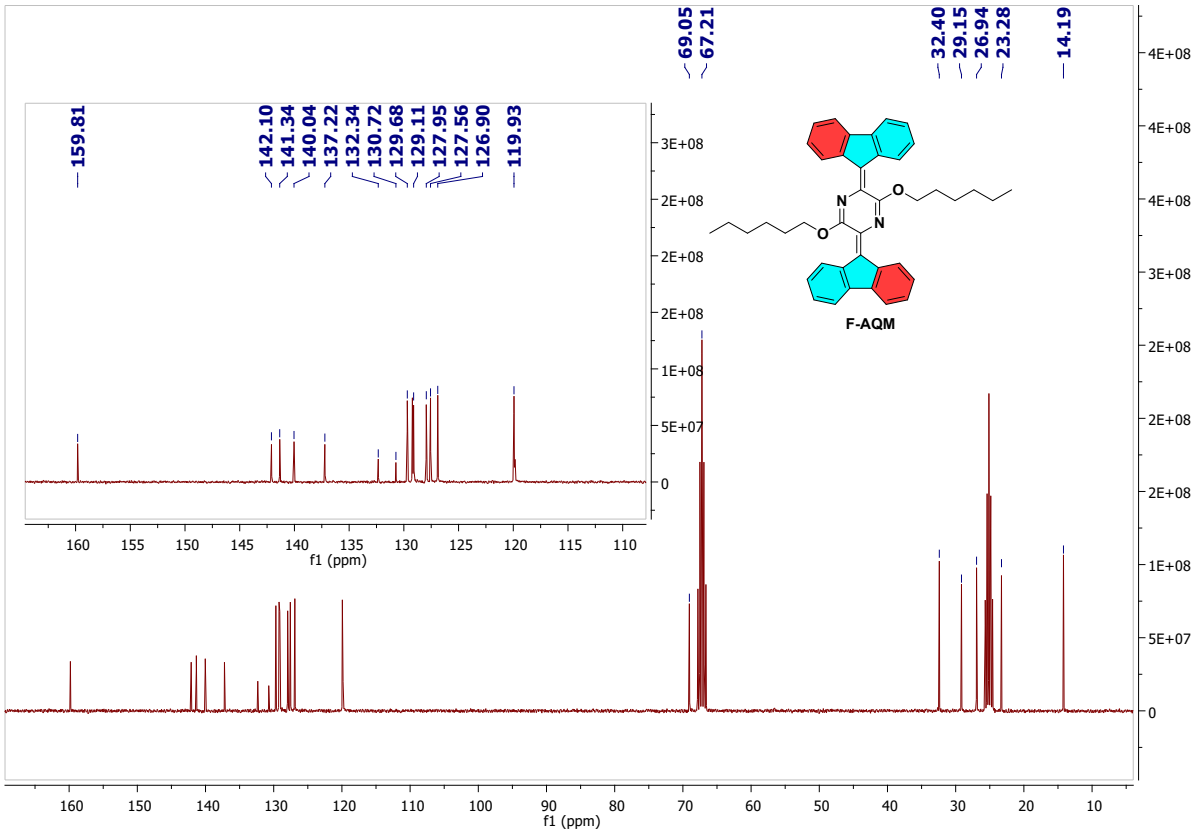

Fig. S21: ^{13}C NMR spectrum of **F-AQM** (THF d_8, 75 MHz)

References

1 P. S. Achanta, B. U. Jaki, J. B. McAlpine, J. B. Friesen, M. Niemitz, S.-N. Chen and G. F. Pauli, *J. Pharm. Biomed. Anal.*, 2021, **192**, 113601.
2 Y. Tang, S. Wang, C. Fang, R. Zheng, P. Xu, J. B. Friesen, S.-N. Chen, Y. Wang, G. F. Pauli and Y. Cheng, *Anal. Chem.*, 2025, **97**, 14220–14229.
3 M. ea Frisch, G. W. Trucks, H. B. Schlegel, G. E. Scuseria, Ma. Robb, J. R. Cheeseman, G. Scalmani, V. Barone, G. A. Petersson and H. Nakatsuji, *Gaussian 16*, Gaussian, Inc. Wallingford, CT, 2016.
4 S. Grimme, J. Antony, S. Ehrlich and H. Krieg, *J. Chem. Phys.*, 2010, **132**, 154104.
5 S. F. Boys and F. and Bernardi, *Mol. Phys.*, 1970, **19**, 553–566.
6 J. Contreras-García, E. R. Johnson, S. Keinan, R. Chaudret, J.-P. Piquemal, D. N. Beratan and W. Yang, *J. Chem. Theory Comput.*, 2011, **7**, 625–632.
7 T. Lu and F. Chen, *J. Comput. Chem.*, 2012, **33**, 580–592.
8 W. Humphrey, A. Dalke and K. Schulten, *J. Mol. Graph.*, 1996, **14**, 33–38.
9 W. Zwaihed, F. Maurel, M. Kobeissi and B. Schmaltz, *Molecules*, 2024, **29**, 186.
10 C. L. Anderson, H. Li, C. G. Jones, S. J. Teat, N. S. Settineri, E. A. Dailing, J. Liang, H. Mao, C. Yang, L. M. Klivansky, X. Li, J. A. Reimer, H. M. Nelson and Y. Liu, *Nat. Commun.*, 2021, **12**, 6818.
11 S. F. Boys and F. and Bernardi, *Mol. Phys.*, 1970, **19**, 553–566.